Resonance as a measure of pairing correlations in the high-T_c superconductor $YBa_2Cu_3O_{6.6}$

Pengcheng Dai*, H. A. Mook*, G. Aeppli†, S. M. Hayden‡ & F. Doğan§

* *Oak Ridge National Laboratory, Oak Ridge, Tennessee 37831-6393, USA*
† *NEC Research Institute, Princeton, New Jersey 08540, USA*
‡ *H. H. Wills Physics Laboratory, University of Bristol, Bristol BS8 1TL, UK*
§ *Department of Materials Science and Engineering, University of Washington, Seattle, Washington 98195, USA*

One of the most striking properties of the high-transition-temperature (high-T_c) superconductors is that they are all derived from insulating antiferromagnetic parent compounds. The intimate relationship between magnetism and superconductivity in these copper oxide materials has intrigued researchers from the outset[1–4], because it does not exist in conventional superconductors. Evidence for this link comes from neutron-scattering experiments that show the unambiguous presence of short-range antiferromagnetic correlations (excitations) in the high-T_c superconductors. Even so, the role of such excitations in the pairing mechanism for superconductivity is still a subject of controversy[5]. For $YBa_2Cu_3O_{6+x}$, where x controls the hole-doping level, the most prominent feature in the magnetic excitation spectrum is a sharp resonance (refs 6–11). Here we show that for underdoped $YBa_2Cu_3O_{6.6}$, where x and T_c are below their optimal values, modest magnetic fields suppress the resonance significantly, much more so for fields approximately perpendicular to the CuO_2 planes than for parallel fields. Our results indicate that the resonance measures pairing and phase coherence, suggesting that magnetism plays an important role in high-T_c superconductivity. The persistence of a field effect above T_c favours mechanisms in which the superconducting electron pairs are pre-formed in the normal state of underdoped copper oxide superconductors[12–14], awaiting transition to the superconducting state.

Neutrons carry magnetic dipoles that are scattered by the electron spins in the sample with a probability—dependent on the neutron direction and energy—directly proportional to the Fourier transform in space and time of the two-spin correlation function, $S(Q,\omega)$. The wavevector Q and energy $\hbar\omega$ are simply the difference between the momenta and energies, respectively, of the incident and scattered neutrons. $YBa_2Cu_3O_{6+x}$ (denoted as $(123)O_{6+x}$) with x of 0.6 was selected because it is a thoroughly characterized high-T_c superconductor that can be fabricated as the large single crystals required for neutron measurements. Equally important, thermodynamic data indicate that even modest fields have a large effect on the electronic entropy in the superconducting phase[15,16]. Thus, if the electronic entropy changes around T_c are mostly due to spin excitations[11], they must respond to an external magnetic field in qualitatively the same way[17].

The compound $(123)O_{6+x}$ contains pairs of CuO_2 layers separated by charge reservoir layers. We label wavevectors $Q = (q_x, q_y, q_z)$ in units of Å^{-1}as $(H, K, L) = (q_x a/2\pi, q_y b/2\pi, q_z c/2\pi)$ in the reciprocal lattice units (r.l.u.) appropriate for the orthorhombic unit cell, for which the lattice parameters (in Å) are $a = 3.83$, $b = 3.88$ ($\approx a$) and $c = 11.743$ if $x = 0.6$. For $x = 0$, $(123)O_{6+x}$ is an antiferromagnetic insulator where the spin on each Cu^{2+} ion is antiparallel to its nearest neighbours, both in its layer and in the immediately adjacent layer[18]. As the oxygen content x is increased, the material becomes a metal and eventually, near $x = 1$, an excellent high-temperature ($T_c \approx 93$ K) superconductor. At x near 0.6, $(123)O_{6+x}$ is also a good superconductor with T_c reduced to about 60 K. During the evolution from insulator to superconductor, static antiferromagnetism is lost while magnetic (spin) fluctuations centred at the $x = 0$ antiferromagnetic Bragg positions—often referred to[6–11] as $Q_0 = (\pi, \pi)$–persist. For highly doped $(123)O_{6+x}$, the most prominent feature in the spin fluctuation spectrum is a sharp resonance that appears below T_c at an energy of 41 meV (refs 6–8). When scanned at fixed frequency as a function of wavevector, the sharp peak is centred at (π, π) (refs 6–8) and its intensity is unaffected by a 11.5-T field in the *ab*-plane[19]. In our underdoped $(123)O_{6.6}$ ($T_c = 62.7$ K)[9], the resonance occurs at 34 meV and is superposed on a continuum which is gapped at low energies[11]. For frequencies below

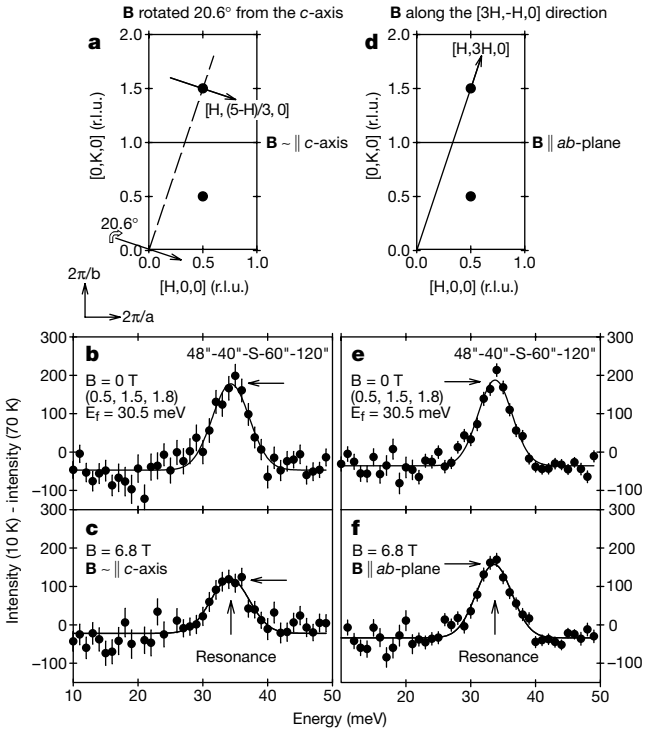

Figure 1 Reciprocal lattice diagram and neutron scattering results. For the experiment, we used the HB-3 triple-axis spectrometer at the High-Flux Isotope Reactor of Oak Ridge National Laboratory. The collimations were, proceeding from the reactor to the detector, 48′-40′-60′-120′ (full-width at half-maximum), and the final neutron energy was fixed at either $E_f = 30.5$ meV or 14.78 meV. The monochromator, analyser and filters were all pyrolytic graphite. The low-temperature data were collected after field cooling the sample from 200 K. **a**, To determine the effect of a field along the *c*-axis on the acoustic spin fluctuations, we first align the crystal in the [*H*, *K*, 0] zone. The sample is then rotated α degrees around the [3*H*, −*H*, 0] direction, where $\alpha = \arctan[(2\pi L/c)/(2\pi\sqrt{(H^2 + (3H)^2)/a})] \approx 20.6°$ for $H = 0.5$ and $L = 1.8$ r.l.u., such that the horizontal scattering plane is spanned by wavevectors along the [1, 3, $\tan\alpha\sqrt{10}\,c/a$] and [3, −1, 0] directions. In this geometry, we can perform both constant-Q (panels **b** and **c**) and constant-energy (Fig. 2a–h) scans at the acoustic-mode intensity maximum ($L = 1.8$ r.l.u.) while still keeping 94% of the applied (vertical) field along the *c*-axis (**B**~||*c*-axis). To see the influence of a field along *c* on the intensity of the optical mode, we oriented the *c*-axis of the crystal perpendicular to the scattering plane (**B**||*c*-axis). This geometry allows any wavevector of form (*H*, *K*, 0), that is, at the $L = 0$ intensity maximum of the optical mode, to be reached. **d**, Conventional [*H*, 3*H*, *L*] zone geometry[8–10] where the applied field is in the *ab*-plane along the [3, −1, 0] direction. **b**, **c**, Difference spectra of the neutron intensities between $T = 10$ K ($< T_c$) and $T = 70$ K ($T_c + 7.3$ K) at wavevector $Q = (0.5, 1.5, 1.8)$ for zero and 6.8-T field in the **B**~||*c*-axis geometry. **e**, **f**, Similar data in the **B**||*ab*-plane geometry. Because of the differences in sample geometries, the actual intensity gain of the resonance in the **B**||*ab*-plane experiment is slightly higher than that of the **B**~||*c*-axis case at zero field for the same incident beam current as measured by monitor (300 monitor counts correspond to ~8 min per point at $\hbar w = 34$ meV). We normalized the intensity gain of the resonance in these two experiments at zero field, and multiplied the finite field case by the same scale factor. Data in Figs 1–4 were obtained from $YBa_2Cu_3O_{6.6}$.

the resonance, the continuum is actually strongest at a quartet of incommensurate positions disposed symmetrically about (π, π) (refs 20, 21). Both the resonance and the incommensurate fluctuations appear in the acoustic channel for the bilayers, meaning that they are due to spin correlations that are antiferromagnetic between the planes. The corresponding neutron-scattering intensities exhibit a modulation $\sin^2(\pi dL/c)$, where d (3.342 Å) is the spacing between the nearest-neighbour CuO_2 planes, along c. In contrast, optical fluctuations are associated with ferromagnetic correlations between planes, and vary as $\cos^2(\pi dL/c)$ along c. The optical fluctuations for $x = 0.6$ have a gap of about 50 meV, well above the acoustic gap of 20 meV (ref. 11).

We mounted the crystal in three different orientations inside a split coil (to provide neutron beam access) 7-T vertical-field superconducting magnet to establish the effects of a field that was orientated in three directions. These directions were approximately along the c-axis (**B**∼‖c-axis, Fig. 1a; to investigate acoustic fluctuations), along the c-axis (**B**‖c-axis; to investigate optical fluctuations), and in the ab-plane (**B**‖ab-plane, Fig. 1d; to investigate acoustic fluctuations). Raw neutron-scattering data for $(123)O_{6+x}$ over the large frequency range covered here contain considerable nonmagnetic background. The background, however, is weakly temperature-dependent for $T < 70$ K, which makes temperature difference spectra a useful guide to the magnetic contributions. Figure 1b shows the effect of superconductivity on $S(Q,\omega)$ at $Q = (1/2, 3/2, 1.8)$ in the form of difference spectra between 10 K ($< T_c$) and 70 K ($T_c + 7.3$ K). At zero field ($B = 0$ T), we reproduce previous results[9] in both the **B**∼‖c-axis (Fig. 1b) and the **B**‖ab-plane (Fig. 1e) sample orientations. The data reveal the positive peak at 34 meV due to the increased resonance amplitude below T_c. Imposition of a 6.8-T field nearly along the c-axis results in the qualitatively similar temperature difference spectrum (Fig. 1c). However, the intensity gain of the resonance is suppressed by ∼30% compared to that at zero field (Fig. 1b). This is remarkable because the magnitude (6.8 T) of the applied field is much less than the upper critical field ($B_{c2} \approx 45$ T) for the material[16], and the corresponding Zeeman (magnetic) energy is, at $\pm g\mu_B B$ (≈ 0.8 meV, assuming the Lande factor $g = 2$ and the resonance measures singlet-to-triplet transition with triplet spin $s = 1$), much smaller than the 34-meV resonance energy and the thermal energy $k_B T_c$ (≈ 6 meV).

In common with other layered superconductors, the thermodynamic properties of the copper oxides are strongly anisotropic with respect to the direction of the applied magnetic field[16]. A field perpendicular to the conducting planes generally causes a stronger suppression of the superconductivity than one applied within the plane. To see whether the resonance intensity depends similarly on field direction, we imposed a 6.8-T field parallel to the ab-plane (Fig. 1f). A noticeable, but much smaller, suppression ($\leq 10\%$) of the resonance is observed. Thus, the anisotropy of the field effect on the resonance reflects the anisotropy of other physical superconducting properties. This is the clearest evidence to date that the resonance is very sensitive to the superconducting pairing.

Although the constant-Q difference spectra (Fig. 1) are excellent for determining the intensity gain of the resonance from the normal to the superconducting state, such measurements do not provide information about how the field affects the momentum distribution of the excitations. We therefore scanned the wavevector in the **B**∼‖c-axis geometry (Fig. 1a) at energy transfers below, at, and above the resonance. At 150 K, the constant-energy scans at the resonance energy (Fig. 2a) show a broad peak centred at (π, π) on a sloped linear background. There are no observable intensity differences in the profiles for $B = 0$ and 6.8 T. On cooling to 70 K (Fig. 2b), the

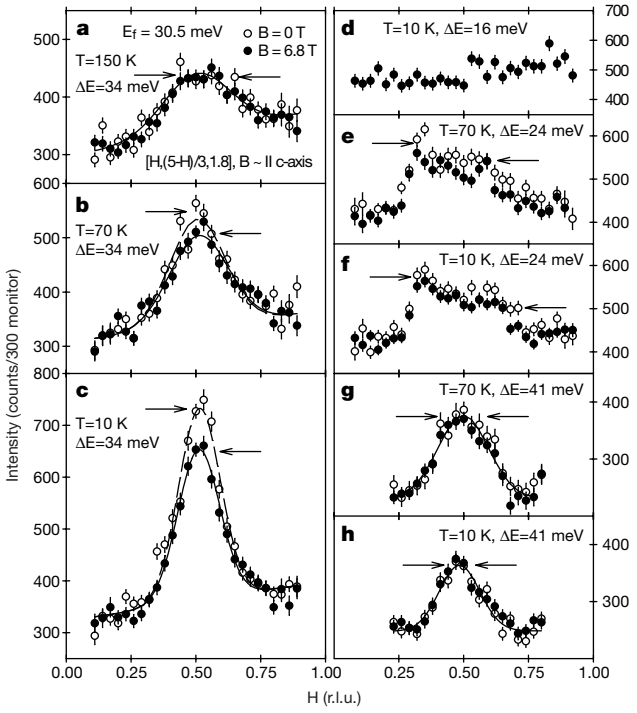

Figure 2 Effect of a magnetic field on the momentum dependence of the spin excitations. The figure shows constant-energy scans of the neutron scattering intensity as a function of wavevector in the **B**∼‖c-axis geometry. **a–c**, Results at the excitation energy of 34 meV; **d**, 16 meV; **e**, **f**, 24 meV; and **g**,**h**, 41 meV. The open and filled circles represent data for identical scans at zero and 6.8-T field, respectively. The dashed and solid lines are gaussian fits to the data.

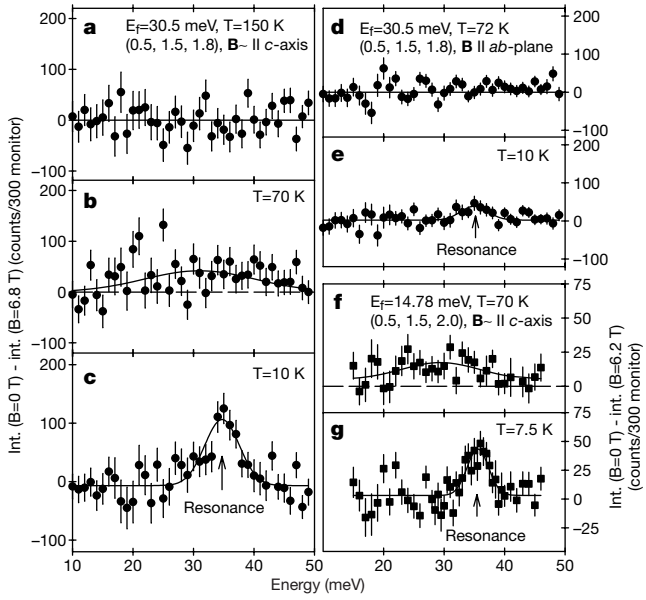

Figure 3 Effect of a magnetic field on the energy dependence of the spin excitations. The figure shows difference spectra of the neutron scattering intensities between zero and finite magnetic field. Panels **a**–**c** and **d**–**e** show the low-resolution results obtained with $E_f = 30.5$ meV at wavevector $Q = (0.5, 1.5, 1.8)$ in the **B**∼‖c-axis and **B**‖ab-plane geometries, respectively. High-resolution measurements in the **B**∼‖c-axis geometry with $E_f = 14.78$ meV are shown in **f** and **g**. The scattering should be centred around zero as shown by the solid lines in **a** and **d** if spin fluctuations are not affected by the field. The solid lines in **c** and **e–g** are unconstrained least-squares fits to the data by gaussians on floating constant backgrounds. The solid line in **b** is a guide to the eye. Positive scattering (above zero) indicates a net loss in the acoustic magnetic spectral weight when the field is applied. Strong phonon scattering at about 20 meV in the raw constant-Q scans yielded the large error bars in the difference spectra around that energy.

resonance narrows in width and grows in intensity, but is also clearly suppressed at 6.8 T. At 10 K (Fig. 2c), the suppression of the resonance at 6.8 T is more severe. Direct inspection and fits of gaussian profiles to the data (Fig. 2a–c) indicate no appreciable field-induced change in the momentum dependence of the resonance peak. In contrast, the thermal fluctuations associated with warming from 10 to 70 K yield a decrease in Q-integrated intensity that is numerically similar to that found on application of a 6.8-T field at 10 K, and makes the profile considerably broader.

Below the 20-meV spin gap in the superconducting state[11], the constant-energy scan at 16 meV in the 6.8-T field (Fig. 2d) is featureless, that is, there are no strong field-induced antiferromagnetic correlations at this energy. At 24 meV, where incommensurate spin fluctuations were observed[20,21], the field seems to suppress the constant-energy profiles in both the normal (Fig. 2e) and the superconducting state (Fig. 2f). The effect is more difficult to see than at the resonance energy, although it could represent a similar fractional change in a considerably smaller signal above background. Finally, when we move to an energy just above the resonance, we discern no field-induced change in the Q-dependent profiles at both 70 K and 10 K (Fig. 2g and h).

To demonstrate the effect of a magnetic field on the energy dependence of the excitations in $(123)O_{6.6}$, we show the experimentally measured difference spectra, $S(Q_0,\omega,B = 0\,\mathrm{T}) - S(Q_0,\omega, B = 6.8\,\mathrm{T})$, for $\mathbf{B}\sim\|c$-axis (Fig. 3a–c) and in the ab-plane (Fig. 3d and e) at different temperatures. As we expect the lattice contribution (phonons) to the scattering to be field-insensitive, this procedure will yield the net change of the magnetic intensity induced by the field. At 150 K, a 6.8-T field has no effect on the spin fluctuations in the measured energy range for $\mathbf{B}\sim\|c$-axis (Fig. 3a). On cooling to 70 K, the difference spectra show a broad peak for $\mathbf{B}\sim\|c$-axis (Fig. 3b) and no discernible feature for $\mathbf{B}\|ab$-plane (Fig. 3d). Higher-resolution measurements in the $\mathbf{B}\sim\|c$-axis geometry at 6.2-T field (Fig. 3f) confirm the result of Fig. 3b. In the superconducting state (Fig. 3c, e and g), the difference spectra show a sharp peak at 34 meV for both field orientations, again confirming that the resonance is the feature most obviously affected by the magnetic field for spin fluctuations below 50 meV. In addition, the sharpness here contrasts with the diffuse nature of the difference just above T_c, thus showing the sensitivity of the resonance width, or decay rate, to true bulk superconductivity even in a material with an extended pseudogap regime above T_c. Simple summation as well as least-squares fits to the data (Fig. 3f and g) indicate that the energy-integrated effect of the magnetic field just above T_c is comparable to that well below T_c. The narrowing of the widths in the field-induced difference spectra together with the approximate preservation of weight in these spectra suggest that the resonance width depends strongly on the phase coherence time, while its integrated weight measures the pair density.

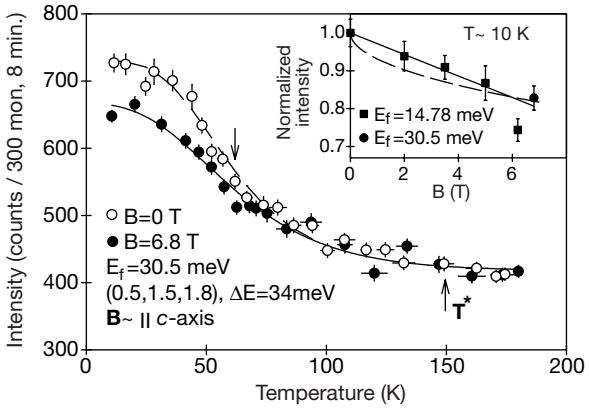

Figure 4 Effect of a magnetic field on the temperature dependence of the resonance and the field dependence of the resonance at about 10 K. The data are collected in the $\mathbf{B}\sim\|c$-axis geometry. The open and filled circles show results at $Q = (0.5, 1.5, 1.8)$ and $\hbar w = 34$ meV for zero and 6.8-T field, respectively. The pseudogap temperature T^* and T_c of the sample are indicated by arrows. The solid and dashed lines are guides to the eye. The inset shows the field dependence of the normalized resonance intensity at approximately 10 K. The filled squares are high-resolution data at $Q = (0.5,1.5,2)$ with $E_f = 14.78$ meV. The solid line corresponds to $I/I_0 = 1 - (B/B_{char})$ with $B_{char} = 36$ T, while the dashed line represents $I/I_0 = 1 - (B/B_{char})^{1/2}$, where $B_{char} = 208$ T.

In Fig. 4 we plot the temperature dependence of the neutron scattering intensity at the resonance energy at zero field and at a field of 6.8 T. Most of the growth in the field-dependent peak signal tracks the growth in the resonance itself on entering the superconducting state. The inset shows the field dependence of the normalized intensity. The solid line is a linear fit to the data—that is, $I/I_0 = 1 - B/B_{char}$ with $B_{char} = 36$ T. Because B_{char} is not far from the upper critical field $B_{c2} = 45$ T estimated for our sample, it is reasonable to associate the sharp resonance peak with the superconducting volume fraction, which for simple superconductors is proportional to $1 - B/B_{c2}$.

Figures 2 and 3 indicate that wherever we look at fixed temperature, the external field either has no effect or reduces the magnetic scattering signal. The total moment sum rule[22,23] states that the magnetic structure factor, when integrated over all wavevectors and energies, should be a temperature- and field-independent constant. Therefore, compensatory increases in signal should occur elsewhere in Q–ω space. Possible destinations for the lost spectral weight include elastic scattering, new or softened optic modes, a subgap continuum, and other continuum scattering spread sufficiently over Q and ω space so as to be unobservable at any particular Q and ω. Searches for the most obvious elastic scattering—that due to the proposed field-induced antiferromagnetic order in copper oxide superconductors[24]—have been fruitless. Scans in the $[H, K, 0]$ plane with $\mathbf{B}\|c$-axis revealed no evidence for optic mode scattering at $\hbar\omega = 34$, 41 and 50 meV apart from that already present at zero field. In addition, we have not yet found field-induced subgap scattering (Fig. 2d). Although our searches for the missing spectral weight were by no means exhaustive, a 6.8-T field does not induce obvious new excitations around (π, π) with energies between 10 and 50 meV that are big enough to compensate the spectral weight loss of the resonance. We note that similar sum rule violations also exist for spectra collected using angle resolved photoemission[25], scanning tunnelling microscopy[26], and infrared spectroscopy[27] in some high-T_c superconductors. However, we point out that an explanation of the superficially similar effects in these measurements must take into consideration the fact that different experimental techniques probe quite different correlations.

We have discovered that a very modest field applied to $(123)O_{6.6}$ yields a very significant reduction in the 34-meV resonance. Therefore, the resonance can be reduced either by warming or applying a magnetic field, with the highest amplitude and narrowest profiles (both in energy and wavevector) occurring in the bulk superconducting state. More surprising is the persistence of the effect above T_c (Figs 2–4). Although there are no explicit microscopic predictions about the effects of magnetic fields on the resonance, our finding has important implications for understanding the mechanism of high-T_c superconductivity. In particular, the larger c-axis field effect presents another challenge to the interlayer tunnelling theory, according to which the resonance should be strongly affected by the in-plane field that disrupts the coherent Josephson coupling along the c-axis[28]. On the other hand, our data are consistent with mechanisms where the dominant loss of entropy on entering the superconducting state is due to the growth of magnetic correlations in the CuO_2 planes[29–31]. A modest field reduces the resonance just as it reduces the specific heat anomaly[15] near T_c, so that the temperature derivative of the resonance intensity tracks the specific heat not only as the hole density is

varied[11], but also as the magnetic field is imposed for fixed x (ref. 17). The anisotropic field effect reflects the anisotropy of other physical properties, such as the magnetic penetration depth and coherence length. Thus, the persistence of the effect above T_c would naturally be due to superconducting fluctuations or incoherent pairing, which also display this anisotropy in the normal state. Such fluctuations exist in models postulating a Bose–Einstein condensation of pre-formed pairs at T_c in the underdoped copper oxides[12–14]. □

Received 16 November 1999; accepted 27 June 2000.

1. Anderson, P. W. The resonating valence bond state in La_2CuO_4. *Science* **235,** 1196–1198 (1987).
2. Emery, V. J. Theory of high-T_c superconductivity in oxides. *Phys. Rev. Lett.* **58,** 2794–2797 (1987).
3. Hirsch, J. E. Antiferromagnetism, localization, and pairing in a two-dimensional model for CuO_2. *Phys. Rev. Lett.* **59,** 228–231 (1987).
4. Schulz, H. J. Superconductivity and antiferromagnetism in the two-dimensional Hubbard model: scaling theory. *Europhys. Lett.* **4,** 609–615 (1987).
5. Scalapino, D. J. The cuprate pairing mechanism. *Science* **284,** 1282–1283 (1999).
6. Rossat-Mignod, J. *et al.* Neutron scattering study of the $YBa_2Cu_3O_{6+x}$ system. *Physica C* **185–189,** 86–92 (1991).
7. Mook, H. A., Yethiraj, M., Aeppli, G., Mason, T. E. & Armstrong, T. Polarized neutron determination of the magnetic excitations in $YBa_2Cu_3O_7$. *Phys. Rev. Lett.* **70,** 3490–3493 (1993).
8. Fong, H. F. *et al.* Phonon and magnetic neutron scattering at 41 meV in $YBa_2Cu_3O_7$. *Phys. Rev. Lett.* **75,** 316–319 (1995).
9. Dai, P., Yethiraj, M., Mook, H. A., Lindemer, T. B. & Doğan, F. Magnetic dynamics in underdoped $YBa_2Cu_3O_{7-x}$: direct observations of a superconducting gap. *Phys. Rev. Lett.* **77,** 5425–5428 (1996).
10. Fong, H. F., Keimer, B., Milius, D. L. & Aksay, I. A. Superconducting-induced anomalies in the spin excitation spectra of underdoped $YBa_2Cu_3O_{6+x}$. *Phys. Rev. Lett.* **78,** 713–716 (1997).
11. Dai, P. *et al.* The magnetic excitation spectrum and thermodynamics of high-T_c superconductors. *Science* **284,** 1344–1347 (1999).
12. Uemura, Y. J. Bose-Einstein to BCS crossover picture for high-T_c cuprates. *Physica C* **282,** 194–197 (1997).
13. Emery, V. J. & Kivelson, S. A. Importance of phase fluctuations in superconductors with small superfluid density. *Nature* **374,** 434–437 (1995).
14. Lee, P. A. & Wen, X. G. Unusual superconducting state of underdoped cuprates. *Phys. Rev. Lett.* **78,** 4111–4114 (1997).
15. Junod, A., Erb, A. & Renner, Ch. Specific heat of high temperature superconductors in high fields at T_c: from BCS to the Bose-Einstein condensation. *Physica C* **317,** 333–344 (1999).
16. Junod, A. in *Studies of High Temperature Superconductors* **Vol. 19** (ed. Narlikar, A. V.) 1 (Nova Science, New York, 1996)
17. Janko, B. Thermodynamic constraints on the magnetic field dependence of the neutron resonance in cuprate superconductors. Preprint cond-mat/9912073 at ⟨http://xxx.lanl.gov⟩ (1999; cited 6 Dec. 1999).
18. Tranquada, J. M. *et al.* Neutron-diffraction determination of antiferromagnetic structure of Cu ions in $YBa_2Cu_3O_{6+x}$ with $x = 0.0$ and 0.15. *Phys. Rev. Lett.* **60,** 156–159 (1988).
19. Bourges, P. *et al.* High magnetic field dependence of spin fluctuations in $YBa_2Cu_3O_7$. *Physica B* **234–236,** 830–831 (1997).
20. Dai, P., Mook, H. A. & Doğan, F. Incommensurate magnetic fluctuations in $YBa_2Cu_3O_{6.6}$. *Phys. Rev. Lett.* **80,** 1738—1741 (1998).
21. Mook, H. A. *et al.* Spin fluctuations in $YBa_2Cu_3O_{6.6}$. *Nature* **395,** 580–582 (1998).
22. Hayden, S. M. *et al.* Absolute measurements of the high-frequency magnetic dynamics in high-T_c superconductors. *Physica B* **241–243,** 765–772 (1998).
23. Aeppli, G. *et al.* The weights of various features in the magnetic spectra of cuprates. *Phys. Status Solidi B* **215,** 519–522 (1999).
24. Arovas, D. P., Berlinsky, A. J., Kallin, C. & Zhang, S. C. Superconducting vortex with antiferromagnetic core. *Phys. Rev. Lett.* **79,** 2871–2874 (1997).
25. Anderson, P. W. Two crucial experimental tests of the resonating valence bond-Luttinger liquid interlayer tunneling theory of high-T_c superconductivity. *Phys. Rev. B* **42,** 2624–2626 (1990).
26. Renner, Ch., Revaz, B., Genoud, J.-Y., Kadowaki, K. & Fischer, Ø. Pseudogap precursor of the superconducting gap in under- and overdoped $Bi_2Sr_2CaCu_2O_{8+\delta}$. *Phys. Rev. Lett.* **80,** 149–152 (1998).
27. Basov, D. N. *et al.* Sum rules and interlayer conductivity of high-T_c cuprates. *Science* **283,** 49–52 (1999).
28. Yin, L., Chakravarty, S. & Anderson, P. W. The neutron peak in the interlayer tunneling model of high temperature superconductors. *Phys. Rev. Lett.* **78,** 3559–3562 (1997).
29. Scalapino, D. J. & White, S. R. Superconducting condensation energy and an antiferromagnetic exchange-based pairing mechanism. *Phys. Rev. B* **58,** 8222–8224 (1998).
30. Demler, E. & Zhang, S. C. Quantitative test of a microscopic mechanism of high-temperature superconductivity. *Nature* **396,** 733–735 (1998).
31. Chakravarty, S. & Kee, H.Y. Measuring condensate fraction in superconductors. *Phys. Rev. B* **61,** 14821–14824 (2000).

Acknowledgements

We thank B. Janko, A. Junod, A. Kapitulnik, M. V. Klein, Ch. Renner and D. J. Scalapino for discussions. The work at ORNL was supported by the US DOE.

Correspondence and requests for materials should be addressed to P.D. (e-mail: piq@ornl.gov).

Quantum correlation among photons from a single quantum dot at room temperature

P. Michler*, A. Imamoğlu*, M. D. Mason†, P. J. Carson†, G. F. Strouse† & S. K. Buratto†

** Department of Electrical and Computer Engineering, and Department of Physics, University of California, Santa Barbara, California 93106, USA*
† Department of Chemistry and Biochemistry, University of California, Santa Barbara, California 93106, USA

Maxwell's equations successfully describe the statistical properties[1,2] of fluorescence from an ensemble of atoms or semiconductors in one or more dimensions. But quantization of the radiation field is required to explain the correlations of light generated by a single two-level quantum emitter, such as an atom, ion or single molecule[3–6]. The observation of photon antibunching in resonance fluorescence from a single atom unequivocally demonstrated the non-classical nature of radiation[3]. Here we report the experimental observation of photon antibunching from an artificial system—a single cadmium selenide quantum dot at room temperature. Apart from providing direct evidence for a solid-state non-classical light source, this result proves that a single quantum dot acts like an artificial atom, with a discrete anharmonic spectrum. In contrast, we find the photon-emission events from a cluster of several dots to be uncorrelated.

The physics of photon antibunching is easy to understand: if a two-level atom emits a photon at time $\tau = 0$, it is impossible for it to emit another one immediately after, because it is necessarily in the ground state. The next photon can only be emitted after a waiting time, which, under weak excitation conditions, is determined by the spontaneous emission time. The result is that there is a dead-time between successive photon-emission events, and the generated photon stream, in the absence of other sources of fluctuation, is sub-poissonian[1]. Photon antibunching is easily washed away with increasing number of atoms. Conversely, we can consider strong photon antibunching as evidence that the source of the radiation field is a single anharmonic (for example, two-level) quantum system: if the spectrum of the emitter is harmonic or there is more than one anharmonic emitter, then the detection of the first

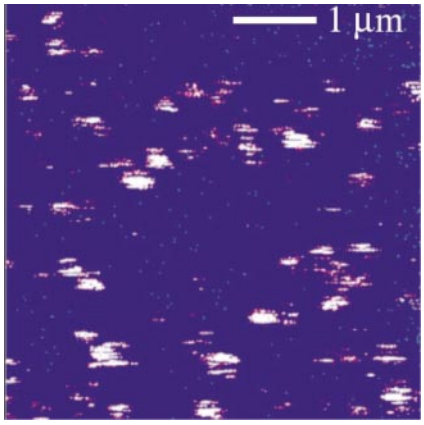

Figure 1 Photoluminescence image of CdSe/ZnS nanocrystals on a glass plate. Image was acquired by raster scanning the particle-covered glass plate through the laser focus ($\lambda = 488$ nm, FWHM was 300 nm) and collecting the photoluminescence onto a single-photon-counting avalanche photodiode. This 256 × 256 pixel image (4.9 ms per pixel) represents an $5 \times 5\ \mu m^2$ field of view.